Angle-resolved line profiles in the predissociation of D_2: A summation of Fano and Lorentzian profiles

Jie Wang[1,2] and Yuxiang Mo[1,*]

[1]*Department of Physics and State Key Laboratory of Low-Dimensional Quantum Physics, Tsinghua University, Beijing 100084, China*

[2]*National Innovation Institute of Defense Technology, Academy of Military Sciences of People's Liberation Army, China, Beijing 100071, China*

(Received 26 October 2021; revised 24 December 2021; accepted 18 January 2022; published 4 February 2022)

Fano profiles usually refer to the line profiles due to the total photon absorption cross sections. In this work, we measured the angle-resolved line profiles of the D($2s, 2p$) fragments from the predissociation of D_2 near the second threshold using the D-atom Rydberg tagging time-of-flight method. The line profiles of the fragments recoiling at the parallel and perpendicular directions to the polarization direction of the excitation laser were found to be significantly different from each other, as well as with the Fano profiles of total absorption cross sections. Based on the previous theoretical results, we found that the angle-resolved line profiles can be expressed as a summation of Fano and Lorentzian profiles. Using the formula and the previously determined parameters from the so-called β profiles, we calculated the angle-resolved line profiles, which are in good agreement with the experimental data. Anisotropy parameters arising from the interferences between the continuum and discrete states were found to play a role in the angle-resolved line profiles.

DOI: 10.1103/PhysRevA.105.023102

I. INTRODUCTION

Fano resonance involves interaction between discrete and continuum states and is ubiquitous in physics [1,2]. The photoexcitation cross sections of the Fano resonance states depend on the interaction strength between the discrete and continuum states, as well as the relative values between the transition dipole moments from the ground state to the continuum state and to the discrete state. The absorption cross sections as a function of excitation photon energies, called as line profile, have asymmetric shapes and are named as Fano or Beutler-Fano profile [3,4]. Fano profiles have been studied using various experimental and theoretical tools [5–13]. It should be emphasized that the Fano resonance is a dynamic process with fragmentation of the parent atom or molecule [1–17]. For example, autoionization processes release free electrons [1]. However, most of the studies of the Fano resonances focused on the total absorption cross sections or the related dynamics, paying much less attention to the differential cross sections as a function of the excitation energies, or the angle-resolved line profiles [11–15]. The angle-resolved measurements pose great challenges to experimentalists, because usually less than 0.1% of the total fragments are collected in the angle-resolved experiments in comparison with those measuring the total absorption cross sections.

For photoexcitation processes, the polarization direction of light defines a direction in space. The fragments recoiling at different angles relative to the polarization direction of the excitation laser may reveal different aspects of the excitation dynamics (henceforth, the recoil direction or angle refers to the polarization direction of the excitation laser), for example, the fragments recoiling at the angles of 0° and 90° mainly reflect the dynamics of parallel and perpendicular transitions, respectively. The angle-resolved line profiles, therefore, are expected to be different for fragments recoiling at different angles if electronic excited states of different symmetries are involved. It is interesting to know if the angle-resolved line profiles could still be described by the Fano formula of total absorption cross sections or be predicted using some parameters related to the Fano profiles and fragment angular distributions.

We have previously reported a measurement of angle-resolved line profiles of the H($2s, 2p$) atoms from the predissociation of H_2 of the $R(0)$ and $R(1)$ transitions in $3p\pi D\,^1\Pi_u^+(\upsilon = 4) \leftarrow X\,^1\Sigma_g^+(\upsilon'' = 0)$ [14]. The line profiles of the H($2s, 2p$) fragments recoiling at angles of 4° and 84° were measured. The Fano formula was found to provide good fits to the two angle-resolved line profiles with two different Fano q parameters. However, the determined Fano q parameters from the fits could not be related to each other or to the Fano parameters of the total absorption cross section, and their relationships were difficult to understand.

About theoretical studies, an analytical expression of differential cross sections as a function of excitation photon energies was previously derived for the predissociation of diatomic molecules using an approximate quantum treatment [12,13]. According to this formula, the angle-resolved line profiles cannot be separated into a product of two functions: angular part and line profile without angular parameter. Therefore, the line profiles of fragments may have different shapes at different recoiling angles. A concise expression of angle-resolved line profile should be derived based on the formula

*Corresponding author: ymo@mail.tsinghua.edu.cn

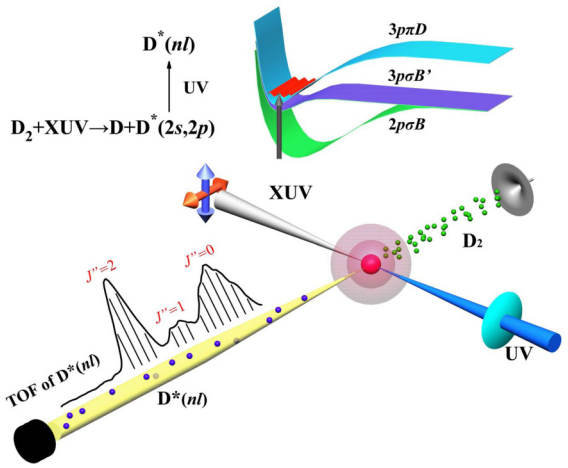

FIG. 1. Schematic diagram of the experimental machine and principle.

of differential cross sections. Unfortunately, such a formula has not been reported and tested with the experimental data.

On the other hand, a formula of anisotropy parameter along the Fano profile, named as the β profile, was derived based on the above-mentioned formula, and was found to be in good agreement with the experimental data. The formula of the β profile was used to extract Fano parameters with good accuracies [13,15].

Here, we report a measurement of the angle-resolved line profiles of the D($2s$, $2p$) fragments from the predissociation of D_2 of the $P(2)$ branch of $3p\pi D\,^1\Pi_u^+(\upsilon = 4) \leftarrow X\,^1\Sigma_g^+(\upsilon'' = 0)$. The line profiles of fragments at 0° and 90° were found to be significantly different. Moreover, both profiles were nicely reproduced using an analytical formula with parameters determined from the recently measured β profiles [14,15]. The results in this work demonstrated that the angle-resolved line profiles can be represented as a summation of a Fano and a Lorentzian profile.

II. EXPERIMENTAL METHOD

Figure 1 shows a schematic diagram of our experimental machine. The machine consists of a tunable extreme ultraviolet (XUV) pump laser (83.9–84.0 nm, ~10 nJ/pulse), a UV probe laser (~365 nm, 1 mJ/pulse), and an H-atom Rydberg tagging time-of-flight (TOF) component, which have been described previously [14–21]. The XUV laser was generated by resonance enhanced four-wave sum mixing ($2\omega_1 + \omega_2$) in a pulsed Kr jet using two laser beams. The first laser beam with frequency ω_1 was generated by the frequency tripling of a dye laser, and the $2\omega_1$ was equal to the transition frequency of the Krypton of $4p^5\,(^2P_{1/2})\,5p[1/2]_0 \leftarrow (4p^6)\,^1S_0$ (98855.1 cm^{-1}). The second laser beam (ω_2) was tuned from 494.5 to 495.5 nm. The two dye lasers were pumped by an Nd-YAG laser (repetition rate 20 Hz). The probe UV laser exciting the D($2s$,$2p$) fragments to high Rydberg states of D(nl, $n \sim 60$) was from the frequency doubling of a third dye laser pumped by the second Nd: YAG laser. The D(nl) atoms flying along the molecular beam direction were detected with a flight distance ~53 cm between the laser molecular beam crossing points and the detector, and the detection solid angle was 1×10^{-3} sr. The D(nl) atoms were electric field ionized between a metal mesh and the front of MCP plate with a distance of ~5 mm, and the D^+ ions were detected with a Z-stack microchannel detector. Note that the region between the laser molecular beam crossing point and the metal mesh was under field-free condition [21]. The TOF spectra of the D(nl) atoms were recorded with a multichannel scaler. The polarization of the XUV laser was controlled by rotating the polarization angle of ω_2 using a Frensel $\lambda/2$ rhomb. The polarization direction of the XUV laser is the same as that of ω_2 [22].

Note that in our previous H_2 experiments, the H(nl) atoms were detected at the directions perpendicular to the plane consisting of lasers and molecular beam [14]. Considering the H_2 molecular beam velocities, the H($2s$, $2p$) fragments were recoiled at 4^0 and 84^0 in the center of mass coordinates.

III. THEORETICAL METHOD

For predissociation of diatomic molecules, the dissociation differential cross sections can be written as [12,13]

$$\sigma(\varepsilon,\theta) = \frac{1}{4\pi}\left[\begin{array}{l}\dfrac{q^2-1}{\varepsilon^2+1}[1+\beta_{\rm res}P_2(\cos\theta)]\sigma_{ic} \\ \quad +\dfrac{2q\varepsilon}{\varepsilon^2+1}[1+\beta_{\rm int}P_2(\cos\theta)]\sigma_{ic} \\ \quad +(\sigma_{ic}+\sigma_{nc})[1+\beta_c P_2(\cos\theta)]\end{array}\right], \quad (1a)$$

$$\varepsilon = \frac{2(\omega-\omega_0)}{\Gamma}, \quad (1b)$$

where θ is the recoil angle of the fragment. $P_2(\cos\theta)$ is the second order Legendre polynomial. ω_0 is the resonance center of the line profile, and Γ the linewidth. σ_{ic} and σ_{nc} represent the partial absorption cross sections due to the continuum states interacting and noninteracting with the discrete state, respectively. $\beta_{\rm res}$, $\beta_{\rm c}$, and $\beta_{\rm int}$ are the fragment anisotropy parameters due to the resonance state, the continuum state, and the interference between the discrete state and the continuum state, respectively.

An integration of the spherical polar angles in Eq. (1a) results in the Fano formula

$$\begin{aligned}\sigma(\varepsilon) &= \sigma_{ic}\frac{(q+\varepsilon)^2}{1+\varepsilon^2}+\sigma_{nc} \\ &= (\sigma_{ic}+\sigma_{nc})\left[\gamma\frac{(\varepsilon+q)^2}{1+\varepsilon^2}+1-\gamma\right], \quad (2a)\end{aligned}$$

$$\gamma = \frac{\sigma_{ic}}{\sigma_{ic}+\sigma_{nc}}, \quad (2b)$$

where q is the Fano parameter, and γ is the fraction of absorption cross section due to the interacting continuum relative to that of the total continuum [1].

The angular distribution of the photofragments is usually written as [23]

$$f(\theta) \propto 1+\beta P_2(\cos\theta). \quad (3)$$

The anisotropy parameters β as a function of excitation energies, β profile, can be represented as the following using

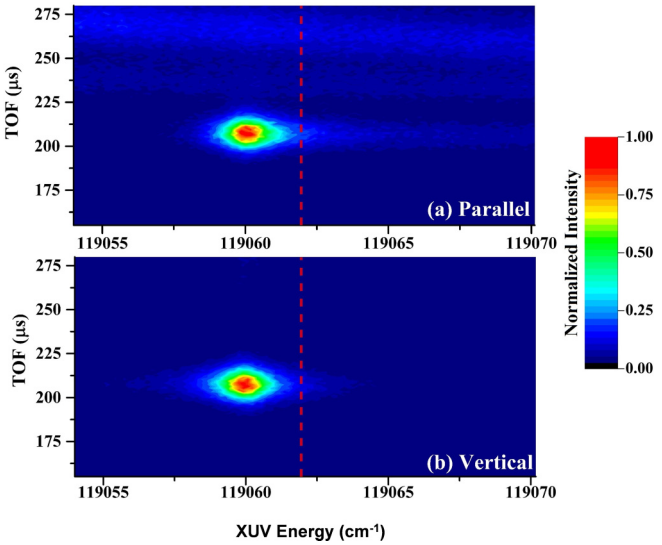

FIG. 2. Two-dimensional pseudocolor contour diagram with the Rydberg tagged D(2*s*,2*p*) atom TOF as the *y* axis and the XUV excitation photon energies as the *x* axis. The D(2*s*, 2*p*) fragments are from the predissociation of D_2 of the *P*(2) branch of $3p\pi D\,^1\Pi_u^+(\upsilon = 4) \leftarrow X\,^1\Sigma_g^+(\upsilon'' = 0)$. The D(2*s*, 2*p*) fragments recoiled from (a) parallel, and (b) perpendicular directions to the polarization direction of XUV laser. TOF spectra along the cuts of the red dashed lines are shown in Figs. 3(a) and 3(b), respectively.

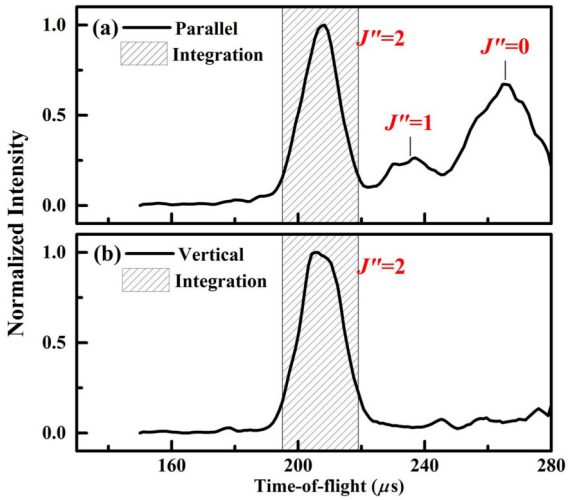

FIG. 3. TOF spectra of the Rydberg tagged D(2*s*, 2*p*) atoms from the predissociation of D_2 with excitation energy at 119062 cm^{-1} along the cuts of the red dashed lines in Fig. 2. The fragment recoil directions were (a) parallel, and (b) perpendicular to the polarization directions of the XUV laser. The integration bounds for determining the angle-resolved line profiles are indicated in the figure.

Eq. (1a):

$$\beta = \frac{\beta_{\rm res}(q^2-1)\gamma + 2q\varepsilon\beta_{\rm int}\gamma + (\varepsilon^2+1)\beta_c}{(\varepsilon+q\gamma)^2 + (1-\gamma)(1+\gamma q^2)}. \quad (4)$$

If $\beta_{\rm res} \neq \beta_{\rm int}$, Eq. (4) results in an asymmetric β profile. The parameters $\beta_{\rm res}$, $\beta_{\rm c}$, $\beta_{\rm int}$, γ, and q in Eq. (4) can be determined by fitting the experimentally measured β profile [13,15].

The expression for angle-resolved line profile, Eq. (1a), can be rewritten in the following form:

$$\sigma(\varepsilon,\theta) = \sigma_c(\theta)\left\{\frac{[\varepsilon+q'(\theta)]^2}{\varepsilon^2+1} + \frac{A(\theta)}{\varepsilon^2+1}\right\}, \quad (5a)$$

$$q'(\theta) = \gamma q\frac{[1+\beta_{\rm int}P_2(\cos\theta)]}{[1+\beta_c P_2(\cos\theta)]}, \quad (5b)$$

$$A(\theta) = \gamma(q^2-1)\frac{1+\beta_{\rm res}P_2(\cos\theta)}{1+\beta_c P_2(\cos\theta)} - q'^2 + 1, \quad (5c)$$

$$\sigma_c(\theta) = \frac{\sigma_{ic}+\sigma_{nc}}{4\pi}[1+\beta_c(\cos\theta)]. \quad (5d)$$

It is seen in Eq. (5a) that the angle-resolved line profile can be represented as a summation of a Fano profile and a Lorentzian curve. The parameter $q'(\theta)$ in Eq. (5b) may be regarded as the modified Fano *q* parameter. The $q'(\theta)$ values are dependent on parameters q, γ, β_c, $\beta_{\rm int}$, and θ. It is obvious that the angle-resolved line profiles are dependent on the fragment recoil angles.

IV. RESULTS

Figure 2 shows the two-dimensional (2D) pseudocolor contour diagram with the TOF of the D(*nl*) atoms as the *y* axis and the XUV photon energies as the *x* axis. Note that the XUV energies were scanned with a step of 0.15 cm^{-1}. Figures 2(a) and 2(b) show the diagrams with the fragments D(2*s*, 2*p*) recoiling at parallel ($0^\circ \pm 1^0$) and perpendicular ($90^\circ \pm 1^0$) directions, respectively. As we mentioned, the D(*nl*) atoms were from the excitation of the D(2*s*, 2*p*) fragments from the predissociation of the *P*(2) branch of $3p\pi D\,^1\Pi_u^+(\upsilon = 4) \leftarrow X\,^1\Sigma_g^+(\upsilon'' = 0)$. Figures 3(a) and 3(b) show the corresponding TOF spectra along the red dashed lines in Figs. 2(a) and 2(b), respectively.

The excitation energy for the TOF spectra shown in Figs. 3(a) and 3(b) is located near the bottom of the line profiles (119062 cm^{-1}). Note that the direct dissociations of D_2 in this energy region are parallel transitions [14–20]. For this reason, there are some background signals in the TOF spectra observed at 0^0 degree [Fig. 3(a)], however, not at 90^0 degree [Fig. 3(b)]. By integrating the signals of $J'' = 2$ in the TOF spectra with proper limits, we obtained the angle- and rotational-resolved line profiles, as show in Figs. 4(a) and 4(b).

It is interesting to see in Figs. 4(a) and 4(b) that the angle-resolved line profile at the parallel direction differs significantly from that at the perpendicular direction. The former has a remarkable asymmetric shape, while the latter is almost a symmetric profile or a Lorentzian. As shown in our previous works on the predissociation of H_2, good fits were possible for the angle-resolved line profiles using the Fano formula [Eq. (2a)] [14]. To examine the changes of the line shapes from recoil angles at 0° to at 90°, we determined their *q* values formally in Eq. (2a) using nonlinear least squares method, they are 9.5 and >30 for the line profiles shown in Figs. 4(a) and 4(b), respectively. The *q* value for the total absorption cross sections (with no angle-resolved) was previously determined as 18.5 ± 0.8 [15,17]. Although the Fano formula is formally good enough to characterize the angle-resolved

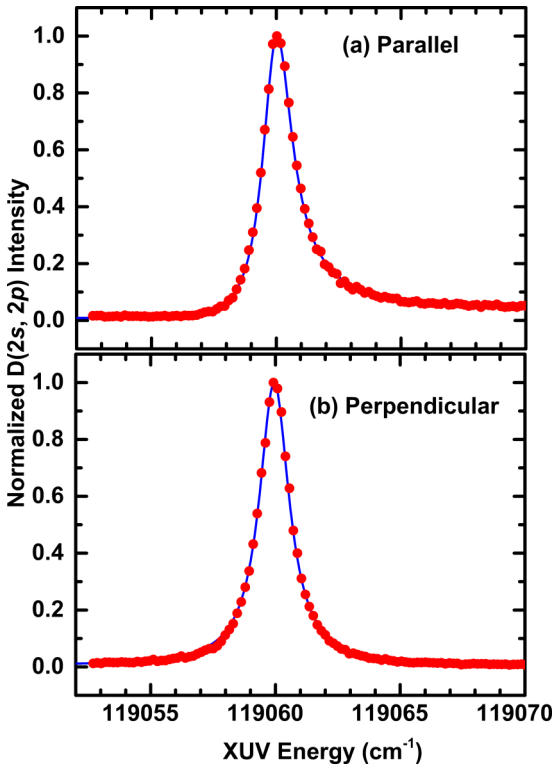

FIG. 4. Recoil angle resolved line profiles of the fragments D(2*s*,2*p*) from the predissociation of the *P*(2) branch in $3p\pi D\,^1\Pi_u^+(\upsilon=4) \leftarrow X\,^1\Sigma_g^+(\upsilon''=0)$ of D_2, in which the fragments recoiled at (a) parallel, and (b) perpendicular directions to the polarization direction of the XUV laser. The spectra were obtained by integrating the signals of $J''=2$ in the TOF spectra. The red dots are the experimental data, and the blue continuous curves are the calculations using Eq. (5a) with parameters listed in Table II.

line shape, the changes of q parameters with the recoil angles are difficult to understand and would need a new way to explain.

As we discussed, Eq. (5a) provides an analytical expression for the angle-resolved line profile. It is noted that the parameters $\beta_{\rm res}$, $\beta_{\rm c}$, $\beta_{\rm int}$, q, and γ for the predissociation of the *P*(2) branch of $3p\pi D\,^1\Pi_u^+(\upsilon=4) \leftarrow X\,^1\Sigma_g^+(\upsilon''=0)$ have been determined in our previous work [15], and are listed in Table I. Using these parameters, the parameters q' and A in Eq. (5a) can be calculated. The angle-resolved line profiles can thus be computed and are shown in Figs. 4(a) and 4(b). It is seen in Figs. 4(a) and 4(b) that the calculations are in excellent agreement with the experimental data.

It would be interesting to know if Eq. (5a) could apply to our previously measured data, angle-resolved line profiles of the H(2*s*, 2*p*) fragments from the predissociation of H_2 of the *R*(0) and *R*(1) transitions $3p\pi D\,^1\Pi_u^+(\upsilon=4) \leftarrow X\,^1\Sigma_g^+(\upsilon''=0)$ [14]. Unfortunately, the parameters $\beta_{\rm c}$, $\beta_{\rm int}$, and γ that are needed to calculate $q'(\theta)$ and $A(\theta)$ in Eqs. (5b) and (5c) have not been determined for these transitions. Note that the $\beta_{\rm c}$ and $\beta_{\rm int}$ are anisotropy parameters and should only depend on the symmetric properties of the related transitions. An analytical expression of γ shows that this parameter also only depends on the initial and final rotational angular momenta of the parent molecule and their projections on the molecular axis [13]. Therefore, in the calculation of the angle-resolved line profiles for H_2, we assumed that $\beta_{\rm c}$, $\beta_{\rm int}$, and γ are the same as those of D_2 with the same type of transitions, which we recently determined [15]. Based on this assumption, we calculated angle-resolved line profiles, and the results are shown in Fig. 5, which are in good agreement with the experimental results.

V. DISCUSSION

The predissociation mechanism of H_2 in the $3p\pi D\,^1\Pi_u$ state is well known [3,14–20,24–35]. The H_2 molecule dissociates via two possible pathways: (a) direct dissociation via the vibrational continuum of the $3p\sigma B'^1\Sigma_u^+$ state, and (b) the molecule is firstly excited to the bound state $3p\pi D\,^1\Pi_u$ and decays via the coupling with vibrational continuum of the $3p\sigma B'\,^1\Sigma_u^+$ state.

Based on the predissociation mechanism of the $3p\pi D\,^1\Pi_u$ state, it may conclude that the fragments measured at different recoil angles would correlate to different dissociation pathways in some way. For fragments recoiling at the parallel direction, a large percentage of the dissociations should occur via the direct dissociation or the pathway (a). However, pathway (b) should also play a role, the two pathways interfere and a typical Fano profile should appear, as shown in Figs. 4(a), 5(a), and 5(b). For fragments recoiling at perpendicular direction, the excitation intensities to the vibrational continuum of the $3p\sigma B'\,^1\Sigma_u^+$ state should be weak, and the excitations should be mainly due to pathway (b). In this case, the determining step of the predissociation is the excitation

TABLE I. Parameters in Eqs. (5b) and (5c) for calculating the angle-resolved line profiles of the predissociation of H_2 and D_2 in the transitions $3p\pi D\,^1\Pi_u^+(\upsilon=4) \leftarrow X\,^1\Sigma_g^+(\upsilon''=0)$.

‘	Branch	$\beta_{\rm res}$	β_c	$\beta_{\rm int}$	γ	q	Γ (cm^{-1})	ω_0 (cm^{-1})
D_2[a]	*P*(2)	0.39	1.54	2.00	0.24	18.5(8)	1.45	119059.9
H_2[b]	*R*(1)	1.12	1.67	1.84	0.71	−10.2(5)	10.7	121041.0
H_2[b]	*R*(0)	1.95	1.75	2.00	0.88	−14.4(5)	4.50	121062.0

[a]Parameters are from Ref. [15]. However, Γ was adjusted from 1.22 ± 0.15 to 1.45 ± 0.1 cm^{-1} to provide a better fit of the experimental data. The larger line width may be due to the large scan step (0.15 cm^{-1}) used in the present experiment.

[b]Parameters $\beta_{\rm c}$, $\beta_{\rm int}$, and γ are assumed to be the same as those of D_2 of the same transitions in Ref. [15]. Other parameters are from Ref. [14].

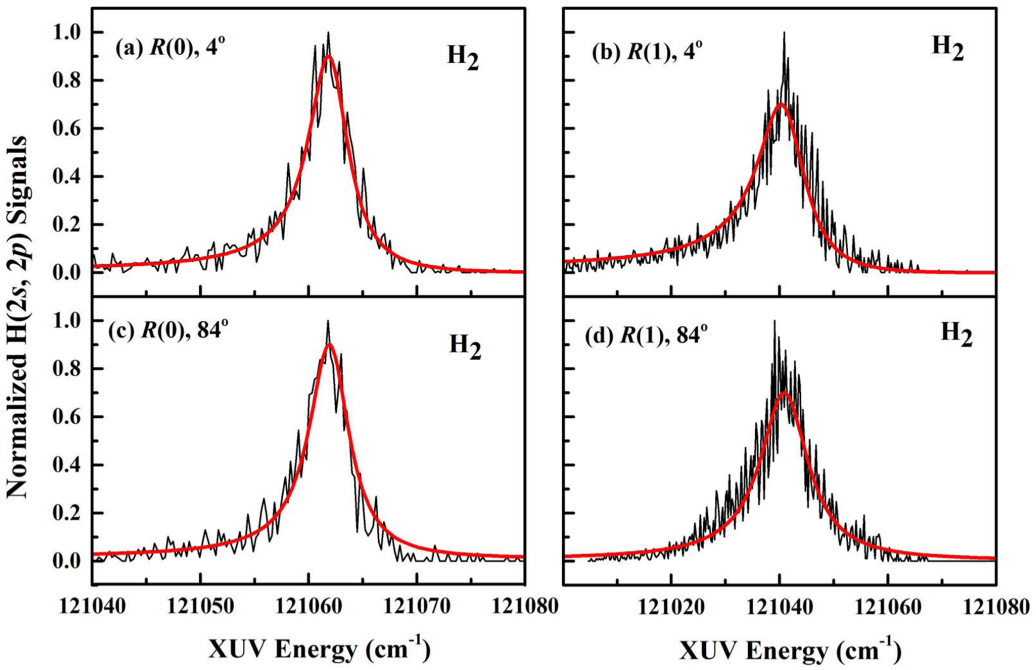

FIG. 5. Recoil angle resolved line profiles of the fragments H($2s$, $2p$) from the predissociations of the $R(0)$ and $R(1)$ branches in $3p\pi D\,^1\Pi_u^+(\upsilon = 4) \leftarrow X\,^1\Sigma_g^+(\upsilon'' = 0)$ of H_2. The fragments recoiled at (a) and (b) 4°, (c) and (d) 84° to the polarization directions of the XUV laser. The rotational branches are indicated in the figures. The fluctuated black curves are the experimental data from Ref. [14], and the smooth red curves are the calculations using Eq. (5a), where the parameters are from Table II.

to the bound state, the measured line profile should like a Lorentzian, as shown by Figs. 4(b), 5(c), and 5(d).

An understanding about the shapes of the angle-resolved profiles can also be gained by studying Eq. (5a). As we mentioned, Eq. (5a) consists of two parts, the first part like a Fano profile, and the second part like a Lorentzian. To examine the relative contributions of the two parts, we have calculated the modified Fano parameters $q'(\theta)$ in the first part and $A(\theta)$ in the second part as a function of angles θ for the $P(2)$ branch of $3p\pi D\,^1\Pi_u^+(\upsilon = 4) \leftarrow X\,^1\Sigma_g^+(\upsilon'' = 0)$ using parameters listed in Table I. The result is shown in Fig. 6. Table II lists the parameters at parallel and perpendicular directions, including the related parameters for H_2.

As seen in Fig. 6 and Table II, when the recoil angles are near 90°, the values of the modified Fano parameters $[q'(\theta)]^2$ are small relative to the $A(\theta)$, and the line profiles approach Lorentzian. In contrast, the values of $[q'(\theta)]^2$ become relatively large at 0^0, and the line profile approach Fano profile. It is also noted that the parameters $A(\theta)$ and $q'(\theta)$ have extreme values for fragments recoiling at 0^0 and 90^0. Therefore, the profiles at 0^0 and 90^0 should not be very sensitive to the angles.

It is also interesting to note that at the so-called magic angle, $\theta = 54.7°$, the line profile has the same form as Eq. (2a) except a constant. Therefore, if we measure the angle-resolved line profiles at the magic angle, we could obtain the Fano profiles of total absorption cross section and determine q, Γ, and ω_0. Furthermore, if we measure the TOF spectra at the magic angle, we can obtain the rotationally resolved Fano profiles by integrating the signals due to a specified rotational state, which is otherwise difficult to measure, and few such spectra have been reported.

There are seven parameters, $\beta_{\rm res}$, $\beta_{\rm c}$, $\beta_{\rm int}$, γ, q, Γ, and ω_0, in the expression for the angle-resolved line profile. Parameters q, Γ and ω_0 are related to Fano profile, which can be determined by measuring the total absorption cross sections or the differential cross sections at the magic angle. $\beta_{\rm res}$ can be determined by tuning the excitation laser to the resonance center. Having determined q, Γ, ω_0, and $\beta_{\rm res}$, the other three parameters, β_c, $\beta_{\rm int}$, and γ could be determined using the

TABLE II. Parameters in Eq. (5a) for the calculation of angle-resolved line profiles in the predissociation of $3p\pi D\,^1\Pi_u^+(\upsilon = 4) \leftarrow X\,^1\Sigma_g^+(\upsilon'' = 0)$[a].

	D_2[b]		H_2			
Parameter	$P(2)$, 0°	$P(2)$,90°	$R(0)$, 4°	$R(0)$,84°	$R(1)$, 4°	$R(1)$ 84°
q'	5.24	0.0	−13.82	−2.70	−7.70	−4.15
A	18.32	287.65	4.75	61.01	−0.19	158.10

[a]Calculated using Eqs. (5b) and (5c) with parameters listed in Table I.
[b]Parameters as a function of angles can be found in Fig. 6.

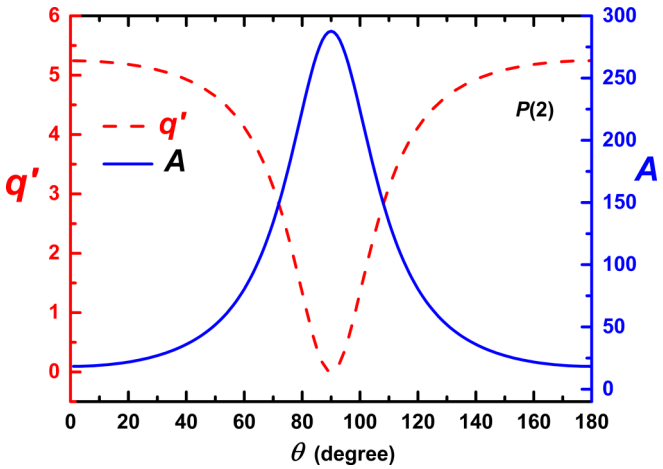

FIG. 6. Parameters $q'(\theta)$ (dashed red line) and $A(\theta)$ (solid blue line) in Eq. (5a) for the $P(2)$ branch in $3p\pi D\,^1\Pi_u^+(\upsilon=4) \leftarrow X\,^1\Sigma_g^+(\upsilon''=0)$ of D_2. Note that $q'(\theta)$ and $A(\theta)$ are associated with the left and right y axes, respectively. Both quantities are dimensionless.

angle-resolved line profiles at 0^0 and 90^0 or other angles with reasonable signal-to-noise ratios. Such kind of experiments are expected to be performed in the future. Note that $\beta_{\rm int}$ is an anisotropy parameter arising from the interference between the discrete state and the continuum state [12,13,15]. As seen in Eqs. (4), (5b), and (5c) and Table I, parameter $\beta_{\rm int}$ plays an essential role in determining the angle-resolved line profile and β profile. It is noted that the parameters, β_c, $\beta_{\rm res}$, $\beta_{\rm int}$, and γ, could also been determined using the β *profiles*. The angle-resolved line profiles and the β *profiles*, in fact, should provide similar information about the photoexcitation dynamics, since they are both derived from Eq. (1a). With all seven parameters measured, we should gain deep insight into the interference dynamics between the discrete and continuum states in the photodissociation.

VI. SUMMARY

We have measured the angle-resolved line profiles for the predissociation of D_2 of the $P(2)$ branch of $3p\pi D\,^1\Pi_u^+(\upsilon=4) \leftarrow X\,^1\Sigma_g^+(\upsilon''=0)$. The line profiles with the fragments recoiling at perpendicular and parallel directions have different shapes, one is near Lorentzian shape and the other has an asymmetric shape. Based on the previous theoretical results [12,13], we found that the angle-resolved line profiles can be expressed as a summation of Fano and Lorentzian profiles. In combination with the previously reported parameters from the β profiles [15], the angle-resolved line profiles were calculated and are in good agreement with the experimental data. In future, the angle-resolved line profiles in combination with the TOF spectra may be used to obtain rotational-resolved Fano profiles. The extension of the present method to autoionization processes may be possible and should be studied in the future.

ACKNOWLEDGMENTS

This work is funded by Projects No. 21773134 and No. 21833003 supported by the National Natural Science Foundation of China, and by Grant No. 2018YFA0306504, supported by the National Key R&D program of China.

[1] U. Fano, Effects of configuration interaction on intensities and phase shifts, Phys. Rev. **124**, 1866 (1961).
[2] A. E. Miroshnichenko, S. Flach, and Y. S. Kivshar, Fano resonances in nanoscale structures, Rev. Mod. Phys. **82**, 2257 (2010).
[3] H. Beutler, A. Deubner, and H.-O. Jünger, Über das absorptionsspektrum des wasserstoffs. II, Z. Phys. **98**, 181 (1935).
[4] H. Lefebvre-Brion and R. W. Field, *The Spectra and Dynamics of Diatomic Molecules: Revised and Enlarged Edition* (Academic Press, New York, 2004).
[5] H. Friedrich, *Scattering Theory* (Springer-Verlag, Berlin, 2016).
[6] M. Wickenhauser, J. Burgdörfer, F. Krausz, and M. Drescher, Time Resolved Fano Resonances, Phys. Rev. Lett. **94**, 023002 (2005).
[7] C. Ott, A. Kaldun, P. Raith, K. Meyer, M. Laux, J. Evers, C. H. Keitel, C. H. Greene, and T. Pfeifer, Lorentz meets Fano in spectral line shapes: A universal phase and its laser control, Science **340**, 716 (2013).
[8] V. Gruson *et al.*, Attosecond dynamics through a Fano resonance: Monitoring the birth of a photoelectron, Science **354**, 734 (2016).
[9] A. Kaldun *et al*, Observing the ultrafast buildup of a Fano resonance in the time domain, Science **354**, 738 (2016).
[10] S. Lee, H. Sun, B. Kim, and K. F. Freed, Vector properties of $S(^3P)$ and $S(^1D)$ in the photodissociation of SH: Quantum interference and overlapping resonance, J. Chem. Phys. **116**, 10656 (2002).
[11] L. D. A. Siebbeles, J. M. Schins, J. Los, and M. Glass-Maujean, Resonance of the $j^3\Delta_g$ state in the differential photodissociation cross section of H_2, Phys. Rev. A **44**, 1584 (1991).
[12] M. Glass-Maujean and L. D. A. Siebbeles, Angular distribution of photofragments along a Fano profile, Phys. Rev. A **44**, 1577 (1991).
[13] L. D. A. Siebbeles and M. Glass-Maujean, Polarization of atomic photofragment fluorescence for excitation along a Fano profile: A quantum-mechanical study, J. Chem. Phys. **101**, 1019 (1994).
[14] Q. Meng, J. Wang, and Y. Mo, Angle-resolved Beutler-Fano profile and dynamics for the predissociation of H_2, Phys. Rev. A **93**, 050501(R) (2016).
[15] J. Wang and Y. Mo, Asymmetry profiles of the fragment anisotropy parameters along the Fano resonances in the photodissociation of H_2, Phys. Rev. A **102**, 050803(R) (2020).
[16] Q. Meng and Y. Mo, Predissociation dynamics in the $3p\pi D\,^1\Pi_u^+(\upsilon=3)$ and $4p\sigma B''\,^1\Sigma_u^+(\upsilon=1)$ states of H_2 revealed by product branching ratios and fragment angular distributions, J. Chem. Phys. **144**, 154305 (2016).

[17] J. Wang, Q. Meng, and Y. Mo, Electronic and Tunneling predissociations in the $2p\pi C\,^1\Pi_u^{\pm}(\upsilon = 19)$ and $3p\pi D\,^1\Pi_u^{\pm}(\upsilon = 4, 5)$ states of D_2 studied by a combination of XUV laser and velocity map imaging, J. Phys. Chem. A **121**, 5785 (2017).

[18] J. Wang and Y. Mo, Isotope effect and gerade versus ungerade symmetry in HD predissociation revealed by the H($2s$), H($2p$), D($2s$), and D($2p$) fragments, Phys. Rev. A **98**, 062509 (2018).

[19] J. Wang, Q. Meng, and Y. Mo, Oscillation of Branching Ratios between the $D(2s) + D(1s)$ and the $D(2p) + D(1s)$ Channels in Direct Photodissociation of D_2, Phys. Rev. Lett. **119**, 053002 (2017).

[20] J. Wang and Y. Mo, Predissociation dynamics of $D_2 + h\upsilon \rightarrow D(1s_{1/2}) + D(2p_{1/2,3/2,}2s_{1/2})$ revealed by the spin-orbit state resolved fragment branching ratios and angular distributions, J. Chem. Phys. **150**, 144306 (2019).

[21] L. Schnieder, W. Meier, and K. H. Welge, Photodissociation dynamics of H_2S at 121.6 nm and a determination of the potential energy function of SH ($A\,^2\Sigma^+$), J. Chem. Phys. **92**, 7027 (1990).

[22] L. Museur, C. Olivero, D. Riedel, and M. C. Castex, Polarization properties of coherent VUV light at 125 nm generated by sum-frequency four-wave mixing in mercury, Appl. Phys. B **70**, 499 (2000).

[23] R. N. Zare and D. R. Herschbach, Doppler line shape of atomic fluorescence excited by molecular photodissociation, Proc. IEEE **51**, 173 (1963).

[24] F. J. Comes and G. Schumpe, Einfluß der rotation auf die lebensdauer prädissoziierender moleküle, Z. Naturforsch. A **26**, 538 (1971).

[25] G. Herzberg, *Topics in Modern Physics: A Tribute to EU Condon* (University Press of Colorado, Boulder, 1971), p. 11.

[26] P. Borrell, P. M. Guyon, and M. Glass-Maujean, H_2 and D_2 photon impact predissociation, J. Chem. Phys. **66**, 818 (1977).

[27] M. Glass-Maujean, J. Breton, and P. M. Guyon, A Fano profile study of the predissociation of $3p\pi D\,^1\Pi_u^+$ the state of H_2, Chem. Phys. Lett. **63**, 591 (1979).

[28] P. M. Dehmer and W. A. Chupka, Predissociation of the $3p\pi D\,^1\Pi_u^+$ state in H_2, HD, and D_2, Chem. Phys. Lett. **70**, 127 (1980).

[29] M. Rothschild, H. Egger, R. T. Hawkins, J. Bokor, H. Pummer, and C. K. Rhodes, High-resolution spectroscopy of molecular hydrogen in the extreme ultraviolet region, Phys. Rev. A. **23**, 206 (1981).

[30] F. Mrugała, Predissociation of the $D\,^1\Pi_u^+$ state of H_2 by photon impact, Mol. Phys. **65**, 377 (1988).

[31] H. Gao, Ch. Jungen, and C. H. Greene, Predissociation of H_2 in $3p\pi D\,^1\Pi_u^+$ the state, Phys. Rev. A **47**, 4877 (1993).

[32] H. Gao, Predissociation of H_2 in the Rydberg states, J. Chem. Phys. **107**, 7278 (1997).

[33] G. D. Dickenson *et al.*, VUV spectroscopic study of the state of molecular deuterium, Mol. Phys. **109**, 2693 (2011).

[34] J. Zs. Mezei, I. F. Schneider, M. Glass-Maujean, and Ch. Jungen, Resonances in photoabsorption: Predissociation line shapes in $3p\pi D\,^1\Pi_u^+ \leftarrow X\,^1\Sigma_g^+$ the system in H_2, J. Chem. Phys. **141**, 064305 (2014).

[35] J. Zs. Mezei, I. F. Schneider, and Ch. Jungen, Multichannel quantum defect theory of photodissociation of H_2, EPJ Web Conf. **84**, 04005 (2015).